INFORMATICS JOURNALS
The Journal of Electrochemical Society of India, *Volume 74, Issue (3&4), April – June 2025; pp. 62–72*
ISSN (Print) : 0013-466X
ISSN (Online) : xxxx-xxxx
DOI: 10.18311/JESCI/2025/51681

Electrodeposition of Ni-V Alloy Coatings for Better Corrosion Protection

Aishwarya S. Suvarna[1] and A. Chitharanjan Hegde[2*]

Electrochemistry Research Laboratory, Department of Chemistry, National Institute of Technology, Surathkal, Srinivasanagar - 575025, Karnataka, India

Abstract

This study reports the electrodeposition of bright and uniform Ni–V alloy coatings from a newly formulated tartrate–sulfate bath containing glycerol as an additive. Deposition parameters were optimised using the Hull cell method over a current density range of 1.0-6.0 A dm^{-2}. Electrochemical behaviour in 3.5% NaCl solution was evaluated by potentiodynamic polarisation and Electrochemical Impedance Spectroscopy (EIS). Results revealed that Ni content in the deposit decreased, while V content increased, with increasing current density, indicating a regular type of codeposition where Ni, being more noble, deposits preferentially. Higher V content was associated with reduced corrosion resistance, with the coating obtained at 1.0 Adm^{-2} exhibiting the lowest corrosion rate. Cyclic Voltammetry (CV) study demonstrated diffusion-controlled deposition, and the presence of glycerol significantly shifted the deposition potential while improving coating brightness. X-Ray Diffraction (XRD) confirmed the formation of a single-phase solid solution of Ni and V across all current densities. The influence of bath composition and current density on coating structure, morphology, and corrosion performance is discussed here.

Keywords: Corrosion Study, Ni-V Alloy, Regular Codeposition, Scanning Electron Microscopy (SEM) Study, XRD

1. Introduction

Among various surface modification techniques, electrodeposition is an effective and versatile method. Electrodeposition is a highly adaptable technique that enables precise manipulation of the deposit's structure and properties by varying the electrolyte composition and processing conditions. As a result, key characteristics such as grain size[1], surface texture[2], roughness[3], hardness[4], wettability[5], and coating thickness[6] can be effectively tuned. In comparison to conventional methods for fabricating Metal Matrix Composites (MMCs), including chemical vapour deposition and mechanical alloying, electrodeposition stands out due to several notable benefits: Fine control over current input[7], operation at relatively low temperatures[8], reduced processing costs[9], minimal energy requirements[10], and ease of scalability for large-scale manufacturing[11]. Moreover, this method supports accurate thickness control and efficient dispersion of nanoparticles, even on components with intricate shapes[12], making it especially suitable for producing dense, complex, and high-precision composite coatings across a wide variety of substrates.

Numerous studies have been reported in the literature concerning the electrodeposition and analysis of zinc-based alloy coatings incorporating iron group metals, specifically Zn-M alloys, where M refers to Ni, Co, or Fe. Moreover, binary alloys like Ni-Co and Ni-Fe have attracted interest due to their improved electrical and magnetic characteristics[13]. Brenner[14] in his seminal treatise on the electrodeposition of alloys of both Zn-based alloys and mutual alloys of Fe-group metals gave an elaborate explanation of the underlying principles and possibilities of codeposition of these metals. He explained one unusual phenomenon encountered in the electroplating of zinc with iron-group metals and Ni-based binary

*Email: acrhegde@gmail.com

alloys, known as anomalous co-deposition. Subsequent research has demonstrated that zinc-iron group metal alloys, as well as their mutual alloys, exhibit enhanced corrosion resistance when contrasted with coatings made from the pure metals alone[15]. In typical electroplating environments, anomalous co-deposition is identified by the predominant deposition of the metal with lower nobility rather than the one with higher nobility. Such a phenomenon is often linked to the suppression of noble metal deposition, due to the formation of hydroxide compounds of the less noble metal at the cathode-electrolyte boundary[16].

Ni-V alloy coatings are of great interest due to their enhanced mechanical and physical properties and were found suitable for various high-temperature applications. Vanadium is added to nickel to improve its yield and tensile strength. In addition, electrodeposited Ni-V alloy coatings are found to be smooth, uniform, with enhanced properties, such as improved hardness, corrosion resistance, and wear resistance, and find various applications. Studies have shown that vanadium-based alloys provide notable benefits compared to other binary alloys when considered for use as structural materials in the first wall or blanket sections of fusion reactors[17]. Vanadium-containing materials are essential in various advanced applications, including aerospace turbine engines, thermal energy generation units, biomedical instruments, nuclear power technologies, and machinery used in industrial chemical and petrochemical operations[18-30]. In addition, Vanadium is a robust refractory metal that significantly improves the mechanical properties of alloys, contributing to increased hardness, enhanced thermal stability, and superior wear resistance[31]. Ni-V coatings are under active investigation for application of catalytic activity[32]. Altering the surface characteristics of metals is a well-established approach to improving their ability to resist corrosion.

Thus, the literature study reveals that compared to the electrolytic development of other Ni-based binary alloy coatings, electrodeposition of Ni-V alloy coatings is reported very little. In addition, not much work is seen in the literature on electrodeposition and characterisation of Ni-V alloy coatings compared to mutual alloys of Fe group metals (like Ni-Fe, Ni-Co, etc.), especially keeping their corrosion resistance as objectives. However, as a rare example, Yoo *et al* reported electrodeposition and characterisation of Co-V alloy coatings. It was shown that V can be co-deposited with Fe group metals, by exhibiting anomalous codeposition behaviour under certain bath parameters[33]. In this direction, the present study introduces a novel Ni-V electrolytic bath to produce bright, uniform coatings of good corrosion resistance. To the best of the authors' knowledge, glycerol has been used first time as an additive in the electrodeposition of Ni-V alloy coatings. The optimisation of bath composition and deposition parameters was carried out using the standard Hull cell technique. Ni-V alloys obtained at different deposition currents were subjected to Energy Dispersive X-ray Spectroscopy (EDS), XRD, and SEM analyses to investigate their composition, structural phases, and morphological characteristics. The experimental findings are interpreted based on the governing principles of alloy deposition.

2. Materials and Methods

A new Ni-V bath has been optimised in terms of its chemical composition and operational parameters using the standard Hull cell technique. Glycerol was used as the additive for the deposition of bright and uniform Ni-V coating. To prepare the electrolyte, high-purity laboratory chemicals were dissolved in distilled water. Table 1 presents the plating bath composition along with the corresponding operating conditions.

2.1 Specimen Preparation

Mild steel specimens (composition: 99.6% Fe, 0.063% C, 0.011% P, 0.03% S, and 0.23% Mn), pretreated using a standard procedure, acted as cathodic electrodes, each exposing a surface area of 7.5 cm^2 to the plating bath. To ensure surface activation, the specimens were immersed in a 10% hydrochloric acid solution before placing them in the electrolyte solution. After coating, the samples were rinsed with distilled water and dried using hot air.

2.2 Electrodeposition of Ni-V Alloy Coatings

The deposition parameters and bath composition for Ni-V alloy coatings were optimised using a standard Hull cell method[34]. The bath composition and operating conditions of the optimised bath are given in Table 1. A variety of Ni-V alloy coatings deposited on the Hull cell panel evidenced that current density (c.d.) has a significant effect on its composition. A bright, smooth and uniform Ni-V coating was developed on the Mild Steel (MS) surfaces, using an optimised bath. Ni-V alloy

Table 1. Bath constituents and operating conditions of the newly proposed Ni-V bath

Bath Ingredients	Composition ($g\ L^{-1}$)	Operating Variables
Nickel Sulphate Hexahydrate ($NiSO_4.6H_2O$)	160.0	Anode: Graphite plate Cathode: Mild Steel Temp: 30 °C pH: 2.5 Current density range: 1.0-6.0 A dm^{-2}
Vanadyl sulfate ($VOSO_4$)	6.6	
Tartaric Acid ($C_4H_6O_6$)	5.0	
L-Ascorbic Acid ($C_6H_8O_6$)	1.3	
Glycerol ($C_3H_8O_3$)	mL/L	

coatings were electroplated and then rinsed with distilled water, air-dried, and stored in a desiccator. Electroplating was carried out in a 250cm^3 PVC plating cell, maintaining a cathode-to-anode distance of approximately 5 cm. Electrodepositions were accomplished using a power source (Model N6705C, Keysight Technologies). For comparison, all coatings were deposited under identical conditions: pH 2.5 ± 0.05), Temperature 30 ± 2 °C, and a fixed deposition time of 10 minutes.

2.3 Electrochemical Study

Corrosion behaviour of the electrodeposited coatings was assessed using both alternating and direct current electrochemical methods. Corrosion resistance behaviour of Ni-V alloy coatings was evaluated by the potentiodynamic polarisation method, and Corrosion Rates (CR) were evaluated by Tafel's extrapolation method with a reproducibility of ± 0.01%. The electrochemical study of electrodeposited alloy coatings was conducted with a VersaSTAT3 system (Princeton Applied Research), and the data were analysed using ZSimpWin for modelling the equivalent electrical circuits. Experiments were conducted using a standard electrochemical setup with three electrodes, employing a 3.5% sodium chloride solution as the corrosive medium. All electrode potentials reported in this work are referenced against a saturated $Hg/HgCl_2/KCl$ electrode. During potentiodynamic polarisation testing, the potential was varied within a ±250 mV range around the Open Circuit Potential (OCP), using a scanning rate of 1.0 mV/s. EIS measurements were performed across frequencies spanning from 100 kHz down to 10mHz, using a sinusoidal excitation signal with an amplitude of ±10mV. The resulting impedance spectra were analysed using ZSimpWin software to simulate an appropriate equivalent electrical circuit. To evaluate the influence of different chemical constituents, including glycerol, on the electrodeposition process, Cyclic Voltammetry (CV) was performed using an electrolyte solution with optimised bath composition. Electrochemical measurements were conducted at a scan rate of 50 mV/s, employing a pure platinum foil (1cm^2) as the counter electrode. Before each measurement, the platinum electrode was cleaned by immersion in a 1:1 solution of nitric acid. CV scans were conducted in quiescent (unstirred) electrolyte, without prior deaeration. The voltage sweep started at 0 V, proceeded in the positive direction, and was then reversed to complete the cycle. The elemental makeup of the coatings was assessed through EDS using an Oxford X-act detector. XRD analysis, performed with a Rigaku MiniFlex 600 using Cu Kα radiation (λ = 1.5418 Å), was used to investigate the composition-dependent crystalline structures of the Ni-V alloy coatings. The corrosion behaviour of electrodeposited alloy coatings developed under different conditions was evaluated using a 3.5% NaCl solution to mimic the harsh marine environment.

3. Results and Discussion

3.1 Cyclic Voltammetry Study

The chemical composition of the electrolyte significantly impacts the electrodeposition mechanism and the resulting coating characteristics. The specific chemical present in the electrolyte solution may influence both the kinetic and thermodynamic behaviour involved in the deposition process, and in some cases, may also modify the electronic properties of the underlying material[35]. In this regard, the CV study provides valuable information about the redox behaviour of a species present in the solution. Hence, the cyclic voltammetry technique was employed to investigate the influence of the complexing species ($C_4H_6O_6$) and the additive ($C_3H_8O_3$) on the electrodeposition behaviour. Cyclic voltammetric measurements were carried out at a scanning speed of 0.1V/s over a potential range extending from ±2000 mV. Cyclic voltammetry was conducted using different bath formulations labelled A, B, C, and D and is shown in Figure 1.

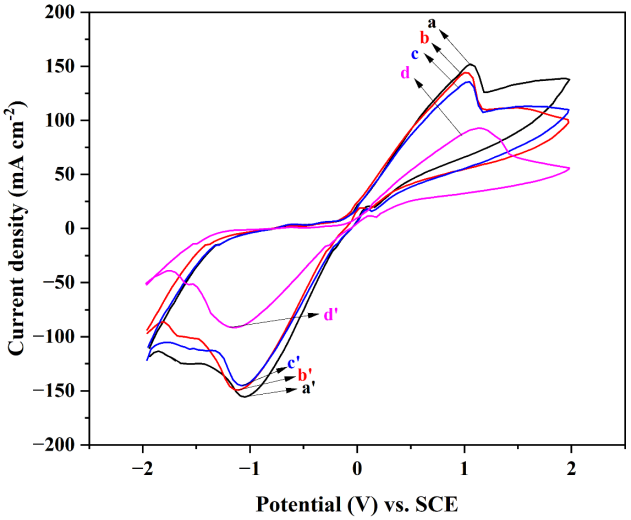


Figure 1. Cyclic voltammograms of Ni-V electrodeposition baths with different formulations: **(a)** $NiSO_4{\cdot}6H_2O$ + $C_4H_6O_6$, **(b)** formulation A + $VOSO_4$, **(c)** formulation B + $C_6H_8O_6$, and **(d)** formulation C + $C_3H_8O_3$, recorded at a scan rate of 100 mV s^{-1} at 30°C.

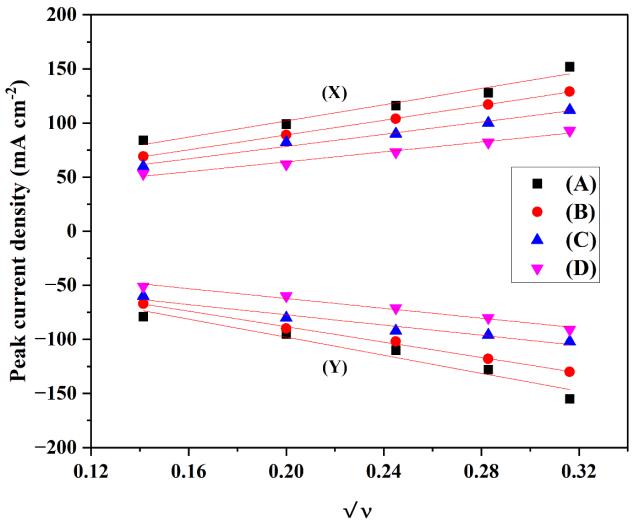


Figure 2. Peak current density versus the square root of the scan rate (√ν) for baths A, B, C, and D at 30°C.

Here, bath A corresponds to $NiSO_4{\cdot}6H_2O$ + $C_4H_6O_6$; bath B corresponds to (A +$VOSO_4$); bath C corresponds to B + L-Ascorbic acid; and bath D corresponds to C+ $C_3H_8O_3$ (additive). The corresponding CV profiles are shown in Figure 1, where curves a, b, c, and d denote anodic peak current densities (ip_a), while a', b', c', and d' indicate cathodic peak current densities (ip_c). As illustrated in Figure 1, the voltammograms reveal significant alterations in the Ni-V alloy deposition behaviour resulting from the incorporation of various components into the electrolyte solution. The changes are seen in both the shape and magnitude of peak current density values of both anodic and cathodic curves, shown as a, b, c, d and a', b', c', d' in Figure 1. A progressive decrease in the anodic peak current (ip_a) values was observed from condition A to D, while the peak potentials (Ep_a) showed a shift toward more positive values, moving from curve 'a to curve 'd. This observed trend suggests that the incorporation of different constituents of the bath, starting from the complexing agent, till the additive has a distinct role in the process of deposition.

The Randles-Sevcik equation, used in cyclic voltammetry, relates the peak current (ip) of a redox reaction to the scan rate (square root of ν), concentration (C) and diffusion coefficient (D) of the electroactive species[36]. It essentially describes how the peak current changes with the scan rate. The equation highlights that faster scan rates lead to larger peak currents (both ip_a and ip_c) due to increased concentration gradients near the electrode. Therefore, to understand the mechanism of deposition, cyclic voltammetry was performed at varying scan rates, specifically 20, 40, 60, and 80mV s^{-1}. This is done to understand the impact of electrolyte constituents on ion transport behaviour near the cathode during electrodeposition. Initially, CV measurements were conducted under bath condition A ($NiSO_4{\cdot}6H_2O$ + $C_4H_6O_6$) at different scan rates, and the corresponding anodic and cathodic peak current densities (ip_a and ip_c) observed were recorded. The study was then repeated for bath formulations B, C and D. Then both peak anodic and cathodic current densities (ip_a and ip_c) against the square root of the scan rate (√ν) were plotted and are shown in Figure 2. A straight-line plot is obtained for both the oxidation and the reduction processes. In addition, graphs associated with both oxidation and reduction for bath formulations from A to D display almost the same slope values. This suggests that during deposition both anodic and cathodic process (shown as X and Y) follows a diffusion-controlled mass transport process, under all conditions of the bath.

3.2 Compositional Analysis

The properties of electrodeposited binary alloy coatings largely depend on the wt.% of individual metals present in them. Therefore, the composition of Ni-V alloy coatings deposited at different current densities was analysed by the EDS method, shown in Figure 3, and the

Table 2. Corrosion data of ED (Ni-V) alloy coatings deposited at different current densities from the optimal bath, with wt. % Ni and V in the deposit.

Current Density (A dm^{-2})	Wt.% Ni in the deposit	Wt. % V in the deposit	$-E_{corr}$ (mV) vs SCE	i_{corr} (µA cm^{-2})	CR × 10^{-2} (mm y^{-1})
1.0	94.6	5.4	263.4	5.22	5.38
2.0	92.6	7.4	494.6	20.24	20.56
3.0	78.5	21.5	614.3	65.67	60.72
4.0	77.6	22.4	631.2	68.29	62.81
5.0	73.5	26.5	664.0	76.51	68.73
6.0	72.0	28.0	704.7	89.88	80.07
Weight % of Ni and V in the bath					
	96.0	4.0			

corresponding data are reported in Table 2. Here, it may be noted that the actual wt.% Ni and V in the deposit are found to be 96.0 % and 4.0 %, respectively.

It was calculated based on the amount of ($VOSO_4$) and $NiSO_4$. $6H_2O$ was taken to prepare the bath. The change in the weight percentage (wt.%) of both Ni and V in the electrodeposited (Ni-V) alloy coatings as a function of current density is shown in Figure 4. Here, wt.% of Ni and V in the bath are shown by horizontal perforated lines, called the composition reference line (CRL) of Ni and V were abbreviated respectively as CRL_{Ni} and $CRL_{V.}$ In the context of electrodeposition of the present Ni-V alloy coating, from the quick reflection on the principle of alloy deposition, it may be noted that the current optimal bath follows a regular type of codeposition. The regular type of codeposition was characterised by the fact that the more readily metal (noble metal deposits preferentially over the less noble metal. This regular codeposition is commonly observed in the co-deposition of two or more iron-group metals (Fe, Co, and Ni), depending on the electrolyte composition and operating conditions. Therefore, in the present Ni-V alloy electrodeposition, more noble Ni (E^0 = - 0.25V) is found to deposit preferentially over the less noble V (E^0 = -1.18V). Figure 4 clearly illustrates that Ni content in the deposit decreases as the current density increases. Further, it may be noted that the Ni content of the alloy remains below the composition reference line (CRL_{Ni}) across all current densities. Conversely, wt.% of V in the deposit increases with current density well above the composition reference line of V (CRL_V).

Hence, the observed reduction in Ni content with rising current density can be explained by a fundamental

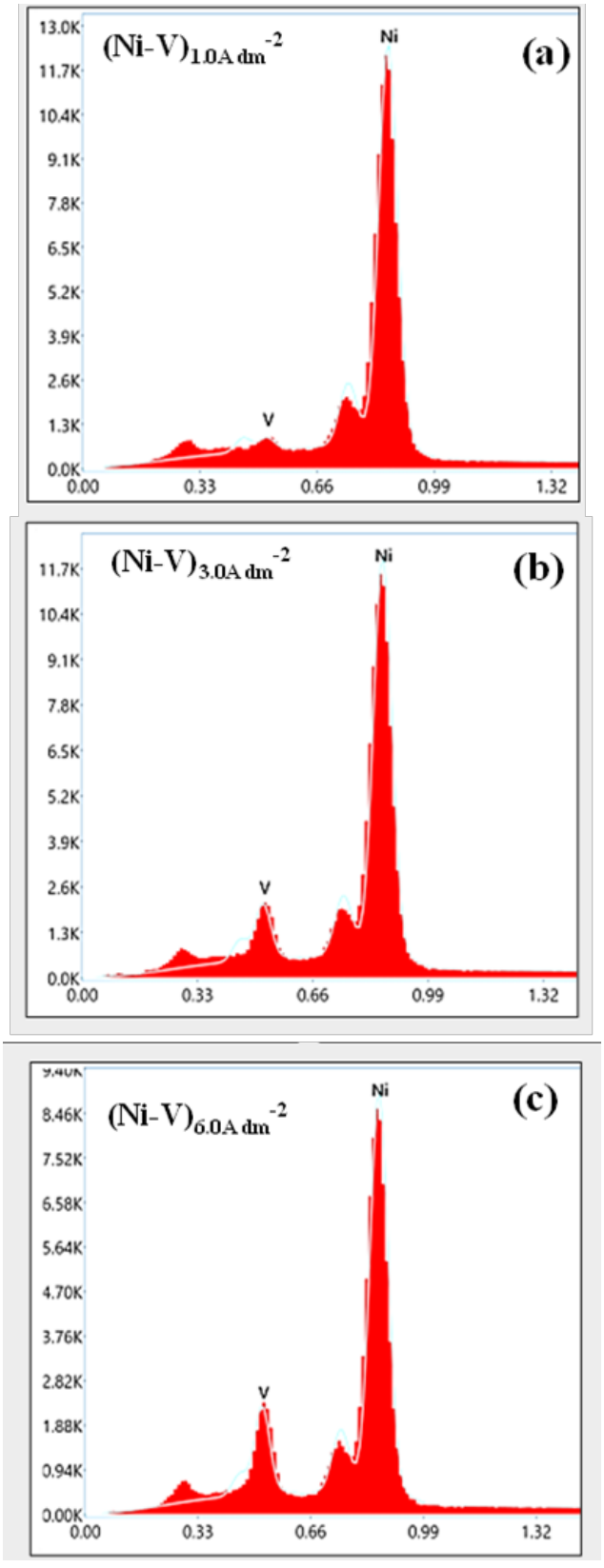


Figure 3. EDS spectra of Ni-V alloy coatings deposited at different current densities from the optimised bath at 30°C.

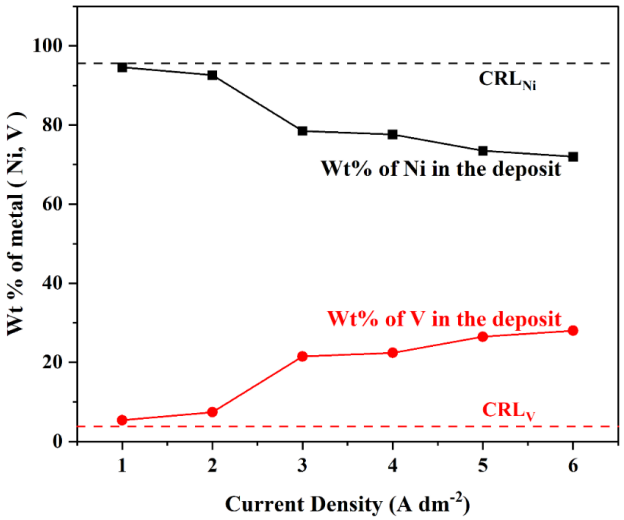


Figure 4. Variation in the wt.% of Ni and V in the deposited alloy as a function of applied current density.

principle of alloy electrodeposition, which states that the deposition rate of the nobler metal tends to decline when plating parameters are modified, such as by lowering agitation, bath temperature, or metal ion concentration, or by increasing the applied current. This suggests that such operating conditions reduce the availability of easily depositable Ni^{2+} ions within the cathodic diffusion zone, leading to a lowered nickel concentration in the resulting coating. Thus, the composition study of Ni-V alloy coatings, deposited at different current densities, justifies that the optimised bath follows a regular type of co-deposition[14].

3.3 Surface Morphology

Generally, during electrodeposition, current density plays an important role in the compactness of the coatings. In general, higher current densities tend to lead to finer-grained, more compact coatings, up to a certain limit. But exceeding this limit can result in increased surface roughness, porosity, and even cracking due to factors like hydrogen evolution and faster deposition rates. Therefore, to understand the morphological change of Ni-V alloy coatings with current density, a SEM study was undertaken. Figure 5 represents SEM micrographs

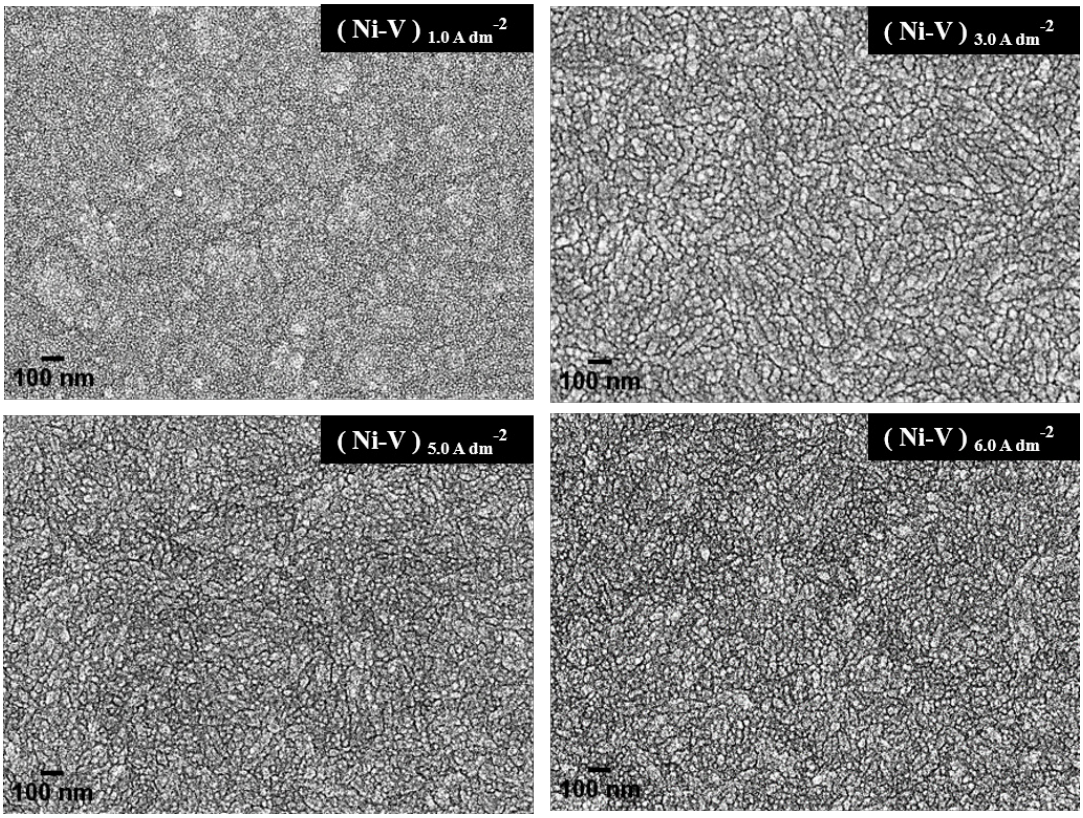


Figure 5. Scanning electron microscopy (SEM) images of Ni-V alloy coatings electrodeposited at different current densities from the optimal bath at 30°C.

of Ni-V coatings formed under varying current density conditions. Surface morphology analysis reveals a strong correlation between the applied current density and the compositional texture of the Ni-V deposits.

Based on the fundamental concepts of electrodeposition, at higher current density, due to a higher rate of nucleation, a finer-grained deposit, a more compact deposit is formed. Generally, electrodeposition occurs in two interconnected phases: nucleation and growth. Initially, well-defined crystallites begin to form at specific locations across the cathode surface and gradually expand. The processes of nucleation and subsequent growth are typically associated with a unique overpotential known as crystallisation overvoltage[37]. Generally, nucleation imposes a greater overpotential compared to the growth phase, as it demands higher activation energy. Consequently, at lower current densities, nucleation is favoured over crystal growth. Hence, at lower current densities, the coating has become smoother and uniform, as shown in the SEM microstructure in Figure 5. At high current densities, Ni–V coatings became rougher, with more surface irregularities. Thus, the increased roughness of Ni-V alloy coatings at higher current densities can be explained by the crystal growth rate surpassing the nucleation rate, and smooth coatings at lower current densities result from the nucleation rate exceeding the crystal growth rate. Changes in coating consistency with current density result from variations in the relative rates of nucleation and crystal growth. It may also be concluded that the observed roughness of the Ni-V alloy coating towards high current density is due to excessive liberation of hydrogen during deposition, limited by the composition of the bath.

3.4 Phase Structure

The phase structure of Ni-V alloy deposits obtained at various current densities was examined using XRD. The XRD patterns of the Ni-V coatings electrodeposited over the current density range of 1.0 - 6.0 A dm^{-2} are presented in Figure 6. The diffractograms reveal that the intensity of the peak corresponding to different phase angles increases with deposition current density, while diffraction angles remain almost unchanged. This suggests that the Ni-V alloy coatings maintain a single-phase solid solution of V in Ni across the studied range, with no prominent alteration in the overall phase structure. If the increase of peak intensity is attributed to the increase of V content in the deposit with current density, and the splitting of peaks corresponding to 4.0 Adm^{-2} and 6.0 Adm^{-2} (Figure 6) is

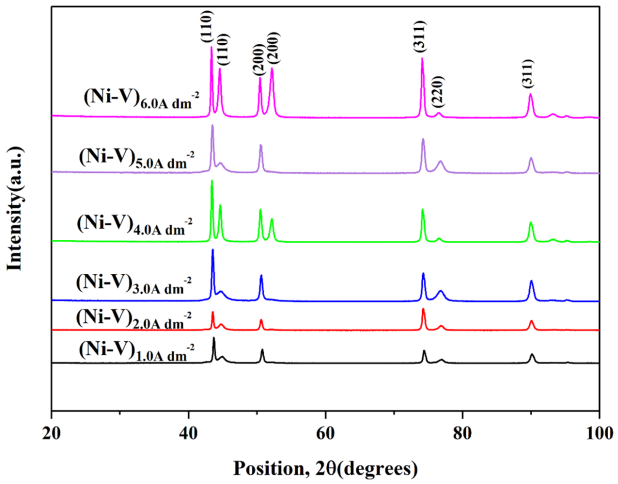


Figure 6. X-ray diffraction (XRD) patterns of Ni-V alloy coatings electrodeposited at different current densities (1.0 6.0 A dm^{-2}), showing peaks corresponding to the fcc phases of Ni and V.

attributed to the change in the relative concentrations of Ni and V rather than the emergence of new crystalline phases. The peak at diffraction angle 43.9°, 50.5°, 75.1°, 90.5° corresponds to the Face Centred Cubic (FCC) structure of (111), (002), (202), and (113) planes of NiV (JCPDS 65-6770) Other peaks at 44.8°, 52.2° and 76.8° are corresponding to (111), (200), and (220) planes of the FCC structure of Ni (JCPDS 03-1051).

3.5 Corrosion Study

The corrosion behaviour of Ni-V alloy coatings electrodeposited at different current densities was studied by electrochemical methods, and experimental results are reported below.

3.5.1 Potentiodynamic Polarisation Study

Corrosion behaviour of Ni-V alloy coatings obtained under varying current densities was evaluated using the Tafel extrapolation technique, wherein both anodic and cathodic polarisation branches were extended to determine the corrosion current density (i_{corr}) value. The corrosion potential (E_{corr}) and corrosion rate (CR) values of Ni-V alloy coatings corresponding to different current densities (1.0 – 6.0 Adm^{-2}) are reported in Table 2, and associated Tafel plots are shown in Figure 7. Analysis of the corrosion parameters and the characteristics of the potentiodynamic polarisation profiles reveals that the Ni-V coating deposited at 1.0 A/dm^2, labelled as $(Ni\text{-}V)_{1.0\ A/dm^2}$, exhibits the lowest i_{corr} value. Hence, $(Ni\text{-}V)_{1.0\ A\ dm^{-2}}$

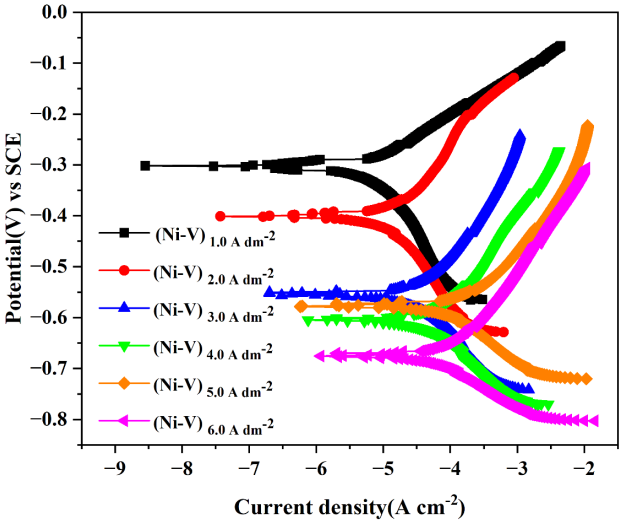


Figure 7. Potentiodynamic polarisation behaviour for Ni-V alloy coatings deposited at different current densities using the optimal bath, using a 3.5% NaCl solution at 30°C.

coating is chosen as the optimal current density of the bath for getting more corrosion-resistant coatings.

3.5.2 EIS Study

EIS was employed to investigate the corrosion behaviour of alloy coatings by analysing charge transfer processes occurring across the electrode-electrolyte interface. In the EIS technique, a small amplitude Alternating Current (AC) of varying frequency from mHz to MHz and corresponding impedance (AC analogue of DC resistance) are measured, and their responses are generally represented as Nyquist and Bode's plots[38]. EIS provides valuable insights into interfacial kinetic parameters of the electrical double layer[39,40]. Nyquist plots are particularly powerful tools in electrochemical analysis, where imaginary impedance (Z_{img}) is plotted against real impedance (Z_{real}) to distinguish between solution resistance (R_s), polarisation resistance (R_p) and other electrochemical parameters.

To gain insight into the protective characteristics of Ni-V coatings formed under various current densities, EIS was conducted, and the corresponding Nyquist plots are presented in Figure 8. It may be noted that all impedance plots shown in Figure 8(a) exhibit a depressed semicircle shape. Such flattened semicircles are typically attributed to surface inhomogeneities, characteristic of alloy coatings which arise due to surface roughness or interfacial effects. The presence of a single semicircular loop in each Nyquist plot suggests that a single charge transfer process dominates

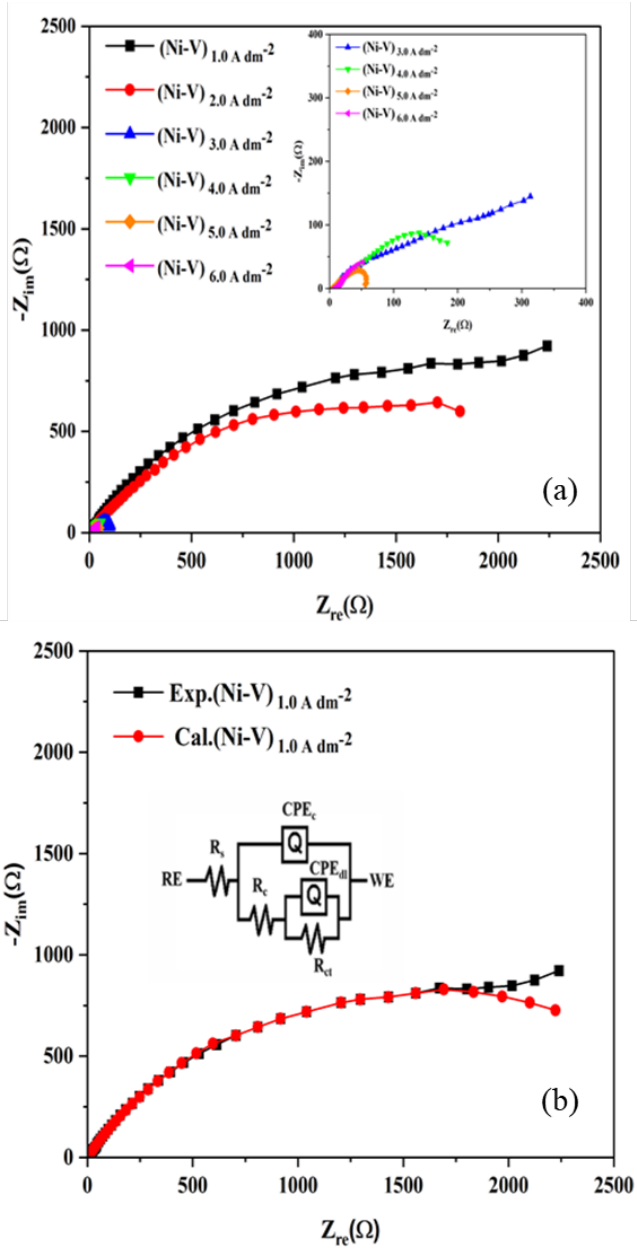


Figure 8. Nyquist plots of electrodeposited Ni-V alloy coatings: **a)** at different current densities (1.0–6.0 A dm^{-2}) from the optimised bath, and **b)** simulation of equivalent electrical circuit (EEC) for Ni-V coating corresponding to optimal current density (1.0 Adm^{-2}).

at the interface. Solution resistance (R_s) shows minimal variation among the coatings, since an identical 3.5% NaCl electrolyte and consistent experimental setup were maintained throughout the investigation. The diameter of the semicircle, which stands for polarisation resistance (Rp) of coatings, is a critical parameter for evaluating their corrosion performance. Hence, Ni–V alloy coating

Table 3. EIS data obtained from equivalent circuit simulation of (Ni-V) alloy coatings electrodeposited at varying current densities from 1.0 to 6.0 A dm^{-2}

Coating Configuration	R_s (Ω)	R_{ct} (Ω)	R_p (Ω)
$(Ni\text{-}V)_{1.0\ A/\ dm^2}$	5.0	3187	3196.5
$(Ni\text{-}V)_{2.0\ A/\ dm^2}$	8.8	1846	1872.1
$(Ni\text{-}V)_{3.0\ A/\ dm^2}$	6.1	257	1043.1
$(Ni\text{-}V)_{4.0\ A/\ dm^2}$	9.0	229	443.5
$(Ni\text{-}V)_{5.0\ A/\ dm^2}$	8.3	169	197.9
$(Ni\text{-}V)_{6.0\ A/\ dm^2}$	8.6	108	117.8

deposited at 1.0 A dm^{-2}, exhibiting the largest capacitive loop (Figure 8a), indicates that it has superior corrosion resistance relative to the other coatings. As polarisation resistance (R_p) is inversely related to corrosion current, the coating obtained at 1.0 A/dm^2 demonstrates the most effective resistance to corrosion among all coatings produced using the same electrolyte formulation.

Further, the electrochemical parameters of impedance study of Ni-V alloy coatings deposited at different current densities are reported in Table 3. It may be noted that Ni-V alloy coating, deposited at 1.0 Adm^{-2} abbreviated as $(Ni\text{-}V)_{1.0}$ Adm^{-2} shows the highest R_p value compared to all other coatings.

The interfacial behaviour of Ni-V alloy coating, deposited at 1.0 Adm^{-2} abbreviated as $(Ni\text{-}V)_{1.0}$ $Adm^{-2,}$ responsible for good resistance, was analysed by modelling an Electrical Equivalent Circuit (EEC). The EEC model provides a reliable framework to interpret the electrochemical characteristics of the coating and to distinguish the resistive and capacitive contributions arising from both the porous structure and the electrochemical interface. The simulated impedance plot of $(Ni\text{-}V)_{1.0}$ Adm^{-2} coating is shown in Figure 8(b) with the equivalent circuit inside. The circuit elements, in addition to the components of the equivalent circuit, indicate the porous nature of the electrodeposited alloy coatings, and comprise the following elements: R_{po} - pore resistance, R_{ct} - charge transfer resistance, C_c - capacitance of the coating and C_{dl} - double layer capacitance responsible for their corrosion resistance performance.

4. Conclusion

In the pursuit of formulating less reported vanadium-based coating systems, a novel sulfate-based electrolyte was developed for the galvanostatic electrodeposition of Ni-V coatings, aiming to enhance the corrosion resistance of mild steel with glycerol as an additive. The following observations were made in conclusion.

1. Bright, sound, and uniform Ni–V alloy coating was successfully developed from a newly formulated sulfate–tartrate bath with glycerol additive over a current density range of 1.0–6.0 A dm^{-2}.
2. The decrease in Ni content and corresponding increase in V content with increasing current density confirm that the developed bath follows a regular codeposition mechanism, where the more noble Ni deposits preferentially.
3. Coatings with higher V content exhibited reduced corrosion resistance, as evidenced by both potentiodynamic polarisation and electrochemical impedance spectroscopy, while the coating deposited at 1.0 Adm^{-2} showed the lowest corrosion rate and highest polarisation resistance, attributed to its higher Ni content and compact surface morphology.
4. Glycerol played a significant role in shifting the deposition potential towards more positive values and improving the brightness of the coatings.
5. Cyclic voltammetry study demonstrated a linear relationship between peak current density and the square root of scan rate, confirming a diffusion-controlled deposition process.
6. X-ray diffraction analysis confirmed the formation of a uniform single-phase solid solution of Ni and V across all applied current densities studied.

5. Acknowledgement

Aishwarya S Suvarna expresses her gratitude to the National Institute of Technology Karnataka (NITK), Surathkal, India, for its support in conducting this research in the Department of Chemistry as a full-time researcher.

6. Funding

No funding was provided for this work.

7. References

1. Aliyu A, Gupta A, Srivastava C, Correlation between texture, grain boundary constitution, and corrosion behaviour of Ni-Cu coatings. Metallurgical and Materials Transactions. 2022; A53, 1440-1449. https://doi.org/10.1007/s11661-022-06605-5

2. Sengupta S, Patra A, Jena S, Das K, Das S, A study on the effect of electrodeposition parameters on the morphology of porous nickel electrodeposits, Metallurgical and Materials Transactions. 2018; A 49(3), 920-937. https://doi.org/10.1007/s11661-017-4452-8
3. Raghavendra C, Basavarajappa S, Sogalad I, Saunshi VK, Study on surface roughness parameters of nanocomposite coatings prepared by electrodeposition process. Materials Today Proceedings. 2021; 38, 3110-3115. https://doi.org/10.1016/j.matpr.2020.09.493
4. Wasekar NP, Haridoss P, Seshadri S, Sundararajan G, Influence of mode of electrodeposition, current density and saccharin on the microstructure and hardness of electrodeposited nanocrystalline nickel coatings. Surface and Coatings Technology. 2016; 291, 130-140. https://doi.org/10.1016/j.surfcoat.2016.02.024
5. Yue B, Zhu G, Wang Y, Song J, Z. Chang N, Guo N, Xu M. Research on wettability of nickel coating changes induced in the electrodeposition process. Journal of Electroanalytical Chemistry. 2022; 910, 116146. https://doi.org/10.1016/j.jelechem.2022.116146
6. Yue B, Zhu G, Wang Y, Song J, Chang Z, Guo N, Xu M. Uncertainty analysis of factors affecting coating thickness distribution during nickel electrodeposition. Journal of Electroanalytical Chemistry. 2021; 891, 115274. https://doi.org/10.1016/j.jelechem.2021.115274
7. Larson C, Farr J, Current research and potential applications for pulsed current electrodeposition - A review. Transactions. 2012; 90, 20-29. https://doi.org/10.1179/174591912X13238641755178
8. Lincot D. Electrodeposition of semiconductors. Thin Solid Films. 2005; 487(1-2), 40-48. https://doi.org/10.1016/j.tsf.2005.01.032
9. Chen H, Wei Z, Zheng X, Yang S, A scalable electrodeposition route to the low-cost, versatile and controllable fabrication of perovskite solar cells, Nano Energy. 2015; 15, 216-226. https://doi.org/10.1016/j.nanoen.2015.04.025
10. Huang J, Daryadel S, Minary-Jolandan M. Low-cost manufacturing of metal-ceramic composites through electrodeposition of metal into ceramic scaffold, ACS Applied Materials and Interfaces. 2019; 11, 4364-4372. https://doi.org/10.1021/acsami.8b18730 PMid:30615419.
11. Guan T, Lu Y, Wang X, Gilchrist MD, Fang F, Zhang N, Scaling up the fabrication of wafer-scale Ni-MoS_2/WS_2 nanocomposite moulds using novel intermittent ultrasonic-assisted dual-bath micro-electroforming, Ultrason. Sonochem. 2023; 95, 106359. https://doi.org/10.1016/j.ultsonch.2023.106359 PMid:36907100 PMCid: PMC10014294.
12. McGeough J, Leu M, Rajurkar K, De Silva A, Liu Q, Electroforming process and application to micro/macro manufacturing, CIRP Annals – Manufacturing Technology. 2001; 50, 499-514. https://doi.org/10.1016/S0007-8506(07)62990-4
13. Fratesi R, Roventi G, Giuliani G, Tomachuk CR. Zinc-cobalt alloy electrodeposition from chloride baths. Journal of Applied Electrochemistry. 1997; 27, 1088-1094. https://doi.org/10.1023/A:1018494828198
14. Brenner A. Electrodeposition of alloys. principle and practice. Academic Press, New York and London, 1963. band i: general survey, principles, and alloys of copper and of silver. 714 S. Mit 212 Bildern Und 45 Tab. DIN A5. Preis: $ 24.-. Berichte der Bunsengesellschaft für physikalische Chemie 1964; 68(3), 309-309. https://doi.org/10.1002/bbpc.19640680319
15. Raveendran MN, Hegde AC, Anomalous codeposition of NiCo alloy coatings and their corrosion behaviour, Materials Today Proceedings. 2022; 62, 5047-5062. https://doi.org/10.1016/j.matpr.2022.02.361
16. Shetty AR, Hegde AC, Effect of magnetic field on corrosion performance of Ni-Co alloy coatings, Journal of Bio- and Tribo-Corrosion. 2022; 9(1). https://doi.org/10.1007/s40735-022-00734-5
17. Smith DL, Loomis BA, Diercks DA, Vanadium-base alloys for fusion reactor applications - A review, Journal of Nuclear Materials. 1985; 135, 125-139. https://doi.org/10.1016/0022-3115(85)90070-4
18. Gorobets OY, Gorobets VY, Derecha DO, Brukva OM. Nickel electrodeposition under influence of constant homogeneous and high-gradient magnetic field. Journal of Physics Chemistry. 2008; C(112), 3373-3375. https://doi.org/10.1021/jp0762572
19. Florea A, Anicai L, Costovici S, Golgovici F, Visan T. Ni and Ni alloy coatings electrodeposited from choline chloride-based ionic liquids: Electrochemical synthesis and characterization. Surface and Interface Analysis. 2010; 42, 1271-1275.
20. Tanaka K, Sakakibara M, Kimachi H, Grain-size effect on fatigue properties of nanocrystalline nickel thin films made by electrodeposition. Procedia Engineering. 2011; 10, 542-547. https://doi.org/10.1016/j.proeng.2011.04.091
21. Ispas A, Matsushima H, Bund A, Bozzini B, A study of external magnetic-field effects on nickel-iron alloy electrodeposition, based on linear and non-linear differential AC electrochemical response measurements. Journal of. Electroanalytical Chemistry. 2011; 651, 197-203. https://doi.org/10.1016/j.jelechem.2010.12.003
22. Rabia J, Tajamal H, Saliha S, Shahid AM, Magnetic field effects on the microstructural variation of electrodeposited nickel film, Material Science and Engineering. A. 1. 2011; 481-487.
23. Aaboubi O. Hydrogen evolution activity of Ni-Mo coating electrodeposited under magnetic field control, International Journal of Hydrogen Energy. 2011; 36, 4702-4709.

https://doi.org/10.1016/j.ijhydene.2011.01.035
24. Rudnik E, Wojnicki M, Wloch G. Effect of gluconate addition on the electrodeposition of nickel from acidic baths. Surface Coating Technology. 2012; 207, 375-388. https://doi.org/10.1016/j.surfcoat.2012.07.027
25. You YH, Gu CD, Wang XL, Tu JP. Electrodeposition of Ni-Co alloys from a deep eutectic solvent, Surface Coating Technology. 2012; 206, 3632-3638. https://doi.org/10.1016/j.surfcoat.2012.03.001
26. Pillai AM, Rajendra A, Sharma AK. Electrodeposited nickel-phosphorous (Ni-P) alloy coating: An in-depth study of its preparation, properties, and structural transitions. Journal of Coatings Technology Research. 2012; 9, 785-797. https://doi.org/10.1007/s11998-012-9411-0
27. Salih SA, Mehdi AS, NouriAlsaegh AS. Study the effect of nickel coating on fatigue life of low-carbon steel exposed to corrosive environments. Journal of Environmental Earth Science. 2013; 3, 121-128.
28. Indyka P, Beltowska-Lehman E, Tarkowski L, Bigos A, Garcia-Lecina E, Structure characterization of nanocrystalline Ni-W alloys obtained by electrodeposition, Journal of Alloys and Compounds. 2014; 590, 75-79. https://doi.org/10.1016/j.jallcom.2013.12.085
29. Wanga S, Guoa X, Yanga H, Daia J, Zhua R, Gonga J, Penga L, Ding W. Electrodeposition mechanism and characterisation of Ni-Cu alloy coatings from a eutectic-based ionic liquid. Applied Surface Science. 2014; 288, 530-536. https://doi.org/10.1016/j.apsusc.2013.10.065
30. Goranova D, Avdeev G, Rashkov R. Electrodeposition and characterization of Ni-Cu alloys. Surface Coatings Technology. 2014; 240, 204-210. https://doi.org/10.1016/j.surfcoat.2013.12.014
31. Wang XG, Sun M, Liu JX, Liu XQ, Ke YB, Jiang WB, Wang H, Fang QF, Wang XP. Effects of vanadium content on the microstructure and tensile properties of NbTiVxZr high-entropy alloys. Journal of Alloys and Compounds. 2024; 987, 174227. https://doi.org/10.1016/j.jallcom.2024.174227
32. Marceta Kaninski MP, Nikolic VM, Tasic GS, Lj. Rakocevic Z. Electrocatalytic activation of Ni electrode for hydrogen production by electrodeposition of Co and V species. International Journal of Hydrogen Energy. 2009; 34, 703-709. https://doi.org/10.1016/j.ijhydene.2008.09.024
33. Yoo BY, Schwartz M, Nobe K. Aqueous electrodeposition of iron group-vanadium binary alloys. Electrochim. Acta. 2005; 50, 4335-4343. https://doi.org/10.1016/j.electacta.2005.01.047
34. Parthasaradhy NV. Practical electroplating handbook, Simon and Schuster, Englewood Cliffs, New Jersey, 1989.
35. Crousier J, Hanane Z, Crousier JP. A cyclic voltammetry study of the Ni-P electrodeposition, Electrochim. Acta. 1993; 38, 261-266. https://doi.org/10.1016/0013-4686(93)85137-N
36. Holze R, Cyclic voltammetry: The complete guide, 1st ed., John Wiley and Sons Ltd., 2025.
37. Kanani N. Electroplating: Basic principles, processes and practice, Elsevier: Burlington, 2005.
38. Yuan XZ, Song C, Wang H, Zhang J. Electrochemical impedance spectroscopy in PEM fuel cells, Springer, London, 2010. https://doi.org/10.1007/978-1-84882-846-9
39. Ciubotariu A, Benea L, Lakatos-Varsanyi M, Dragan V. Electrochemical impedance spectroscopy and corrosion behaviour of Al_2O_3-Ni nanocomposite coatings. Electrochim. Acta. 2008; 53, 4557-4563. https://doi.org/10.1016/j.electacta.2008.01.020
40. Sherif ESM, Erasmus RM, Comins JD. *In situ* Raman spectroscopy and electrochemical techniques for studying corrosion and corrosion inhibition of iron in sodium chloride solutions. Electrochim. Acta. 2010; 55, 3657-3663. https://doi.org/10.1016/j.electacta.2010.01.117